

pubs.acs.org/JACS Article

Synthetic Macrocycle Nanopore for Potassium-Selective Transmembrane Transport

Dan Qiao, Himanshu Joshi, Huangtianzhi Zhu, Fushi Wang, Yang Xu, Jia Gao, Feihe Huang, Aleksei Aksimentiev, and Jiandong Feng*



Cite This: https://doi.org/10.1021/jacs.1c04910



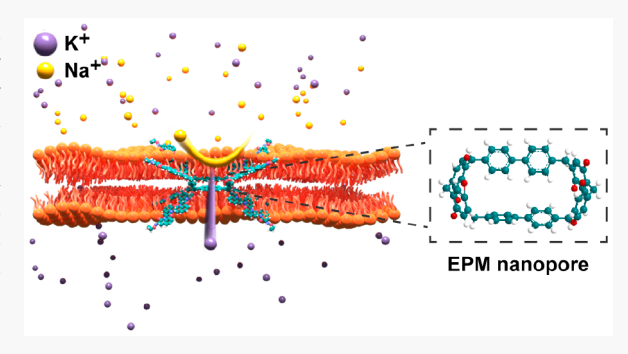
ACCESS

III Metrics & More

Article Recommendations

Supporting Information

ABSTRACT: Reproducing the structure and function of biological membrane channels, synthetic nanopores have been developed for applications in membrane filtration technologies and biomolecular sensing. Stable stand-alone synthetic nanopores have been created from a variety of materials, including peptides, nucleic acids, synthetic polymers, and solid-state membranes. In contrast to biological nanopores, however, furnishing such synthetic nanopores with an atomically defined shape, including deliberate placement of each and every chemical group, remains a major challenge. Here, we introduce a chemosynthetic macromolecule—extended pillararene macrocycle (EPM)—as a chemically defined transmembrane nanopore that exhibits selective transmembrane transport. Our ionic current measurements



reveal stable insertion of individual EPM nanopores into a lipid bilayer membrane and remarkable cation type-selective transport, with up to a 21-fold selectivity for potassium over sodium ions. Taken together, direct chemical synthesis offers a path to *de novo* design of a new class of synthetic nanopores with custom transport functionality imprinted in their atomically defined chemical structure.

INTRODUCTION

Biological membrane channels facilitate transport of ions and water through the barrier of a cell membrane with enormous selectivity, creating and maintaining a transmembrane potential—the fundamental property of a living cell. Guided by several high-resolution atomic structures, biophysics research derived mechanistic understanding of ion conductance and selectivity in potassium channels. The selectivity filter in the biological potassium channel is thought to perfectly coordinate K⁺ ions during the passage, compensating the dehydration energy penalty *via* multiple proposed mechanisms. ^{2,3} On the other hand, *de novo* construction of a highly efficient, stable, artificial potassium channel remains a grand challenge. Creation of such synthetic systems will not only enrich our understanding of ion transport but also enable technological advances in nanopore applications. ^{4–6}

Artificial nanopores have mimicked the basic structure and many functions of natural channels in activated conduction, water transport, biomolecule translocation, and cation—anion selectivity. In contrast to their natural counterparts, in the constellation of heavily explored artificial nanopores such as solid-state nanopores, nanopores in 2D materials, carbon nanotube porins, DNA origami nanopores, and polymer channels, none of these well-established nanopore systems displays considerable potassium selectivity over other monovalent cations at a single nanopore level. Ensemble

measurements, in turn, have identified several groups of synthetic chemical constructs, such as crown ethers and pillararenes, as potential candidates for the construction of artificial potassium channels. Solid-state nanopores functionated with potassium-selective crown ethers were shown to exhibit potassium ion selectivity in both theory and experiment. However, demonstrating intrinsic potassium selectivity of individual synthetic nanopores remains challenging due to the difficultly of unambiguously measuring the ionic currents from individual, stably formed macromolecular nanopores.

■ RESULTS AND DISCUSSION

Inspired by the biological systems, we designed a chemically defined macrocycle nanopore with an ion-conducting cavity that spans a lipid membrane. Our synthetic nanopore was built using pillararene²² derivatives to feature a central cavity decorated with eight peptide chains. Our approach to chemical synthesis was adapted from the previous work used to obtain

Received: May 12, 2021



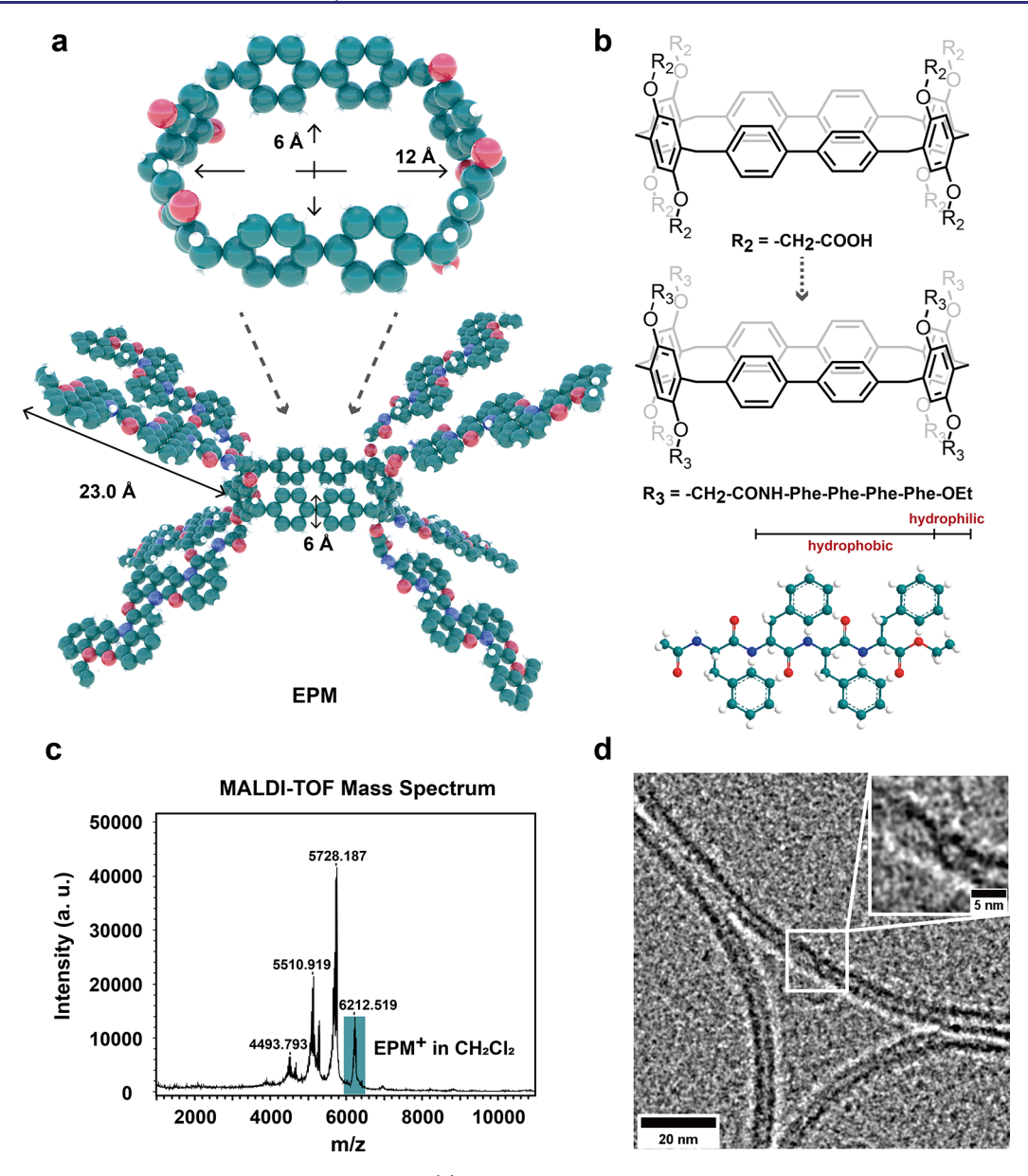


Figure 1. Synthetic nanopores based on the EPM molecules. (a) 3D geometry of the synthetic EPM nanopores. Length of side chain: 23.0 Å. Cavity size: 6 and 12 Å. (b) Peptide side-chain modification process of the EPM nanopores and the structure of peptide side chains. Green: carbon atom. Red: oxygen atom. Blue: nitrogen atom. White: hydrogen atom. (c) MALDI-TOF mass spectrum of the EPM pore. EPM with eight side chains is marked in color shadow. Other m/z peaks may be assigned to EPM with less substituents. (d) Cryo-EM of EPM nanopores on lipid vehicles.

macrocycle molecules²³ (Figures S1 and S2). Each intermediate product of the synthesis process was identified by spectroscopic analysis using ¹H nuclear magnetic resonance (NMR) and a matrix-assisted laser desorption/ionization-timeof-flight mass spectrometer (MALDI-TOF). As shown in Figure 1a, the EPM molecule is composed of four hydroquinone units linked with two biphenyl groups, forming a molecular cavity with an effective diameter of 12 Å along the long axis and 6 Å along the short axis (Figure 1b). To incorporate this structure into lipid membranes, we further designed the side chains²⁴ attached to the EPM ring (Figure S2) to contain four phenylalanine (Phe) units that mediate the adhesion of EPM molecules to lipid bilayers and stimulate the formation of stable transmembrane channels. MALDI-TOF data of the obtained EPM products (Figure 1c, Figure S3) indicate the molecular weight of individual channels of 6212.5

Da, matching the 6214.9 Da molecular weight of the designed structure, which demonstrates the successful modification of the side chains. The lower molecular weight (4000–6000 Da) may be assigned to molecules with less substituents owing to their bulky steric hindrance.

Varying the number of hydroquinone groups at the pore constriction enables precision-tuning control over the size of the central cavity²² (Table 1). As the molecular cavity of EPM is made of only a monolayer of benzene derivatives, its effective thickness is estimated to be 6 Å, comparable to the thickness of single-layer MoS₂ nanopores,¹⁰ though the presence of the side chains may slightly increase the effective thickness. This bottom-up pore-forming approach is analogous to the assembly of DNA origami nanopores.^{12,25,26} Notable advantages of the synthetic approach are the angstrom-precision definition of the nanopore geometry, the uniformity in the

Table 1. Structure of Synthetic Macrocyclic Molecules

| | Molecule | Pillar[8]arene derivatives | Pillar[9]arene | Pillar[10]arene | Pillar[11]arene | Pillar[12]arene |
|----|--------------------------|--------------------------------|----------------|-----------------|-----------------|-----------------|
| | Structure | R R R | | | | |
| 25 | Cavity size(Å) | Short axis: 6 Long axis: 12 | 9.3* | 10.5* | 11.6* | 12.7* |
| | Modification sites (max) | 8 | 18 | 20 | 22 | 24 |

molecular structure among different copies of the nanopore, and the possibility of direct site-specific addition of functional chemical groups.

Spontaneous insertion of nanopores into lipid bilayers is favorable for pore-forming proteins that have hydrophobic surfaces.^{27,28} Hydrophilic nanopores can, nevertheless, be inserted with the help of hydrophobic chemical modifications that outweigh the free-energy penalty for having a hydrophilic molecule inserted in a lipid bilayer. 12,29,30 In our system, we designed the length of the Phe chain (23 Å) to match the width of a lipid bilayer (\sim 40–50 Å) in a fully extended state, as illustrated in Figure 1. The presence of the side chains also prevents the self-assembly of multiple EPM molecules into long supramolecular nanotubes.¹⁷ Although determining the exact spatial arrangements of the pores in the lipid membrane is challenging due to the lack of the characterization resolution, cryo-electron microscopy (cryo-EM) of lipid vesicles mixed with EPM molecules (Figure 1d) suggests the formation of single transmembrane pores and no evidence of intermolecular aggregation (Figure S4).

To demonstrate that the synthetic molecules can form membrane-spanning nanopores, we employed single-channel electrical recording to probe the ionic transport properties. Potassium chloride (KCl) solution containing EPM molecules (Supporting Information) was added to the *cis* chamber, and the transmembrane current was recorded under a bias of 200 mV. In the representative current traces, Figure 2a, we observed a stepwise increase in the ionic current resulting from the successive incorporations of individual EPM nanopores into lipid membranes. The rate of pore insertion could be controlled by dilution of the EPM solution and the voltage magnitude, enabling us to record single-step incorporation events (Figures S5-S7). The single-step conductance histogram, Figure 2b, indicates that the EPM nanopores have an average ionic conductance of 99.28 ± 1.95 pS in 500 mM KCl, as confirmed by the current voltage (I-V) characteristic measurement, Figure 2c. The current traces measured at different ion concentrations, Figure 2d, indicate formation of a stable transmembrane channel (Figure S7), which can last for up to 1 h (Figure S6).

The measured dependence of the ionic conductance (Figure S8) on the ion concentrations further shows that the measured current results from ion permeation across the membrane. The ionic current noise in the EPM nanopores was found to be

similar to that of protein nanopores and increase with ion concentration, as shown by the power spectral density (PSD) analysis (Figure S9). The conductance of single pores is also subject to pH control (Figure S10). A fraction of the pores (~20% of total observations) was found to exhibit a gating behavior that featured a stochastic switching between two conductance states (Figure 2d), similar to gating observed in biological ion channels, DNA origami, and nanotube porins. 12,31 Although the gating baseline stays at the same conductance level as in the stable single channel recordings, the gating phenomenon is hard to control and can originate from a variety of reasons, including structural and charge fluctuations.32

Owing to the pore walls containing π -electron-rich hydroquinones, the cavity of an EPM molecule can directly interact with electron-poor species like cations via the host-guest interactions.³³ To identify the specificity of the supramolecular interaction with different cation types, we measured the transport of sodium ions and potassium ions through a single EPM pore as a function of ion concentration. Strikingly, the *I*– V data presented in Figure 3a and Figure S11 display a clear potassium selectivity: the EPM pore conductance (223.5 ± 22.9 pS) in 1 M KCl is 1 order of magnitude higher than that in 1 M NaCl (22.4 \pm 0.4 pS). To quantify this difference, we used the ratio between the potassium conductance and the sodium conductance as the selectivity factor²¹ (Figure 3b). Similar to natural potassium ion channels,³⁴ the selectivity improves when the ion concentration is increased from 50 mM to 2 M and reaches a factor of 21 at 2 M.

The ion selectivity was further characterized by reversal potential measurements under a concentration gradient condition. As shown in Figure 3c, a reversal potential of −18.0 mV was observed for potassium ions (500 mM KCl/100 mM KCl) in contrast to a -9.5 mV potential measured for sodium ions (500 mM NaCl/100 mM NaCl). Based on the reversal potential and the Goldman-Hodgkin-Katz equation,³² we estimate the ion selectivity of up to 18.9 (condition: 2 M/200 mM), as detailed in Figure S12.

The potassium-selective conductance (Figure 3d) of the same EPM nanopore is found to be reversible, as shown by sequential recordings in the solution replacement experiments (Figure S13). That is, favorable potassium conduction is restored when the solution is changed back to KCl. The observed potassium selectivity can be explored to design new

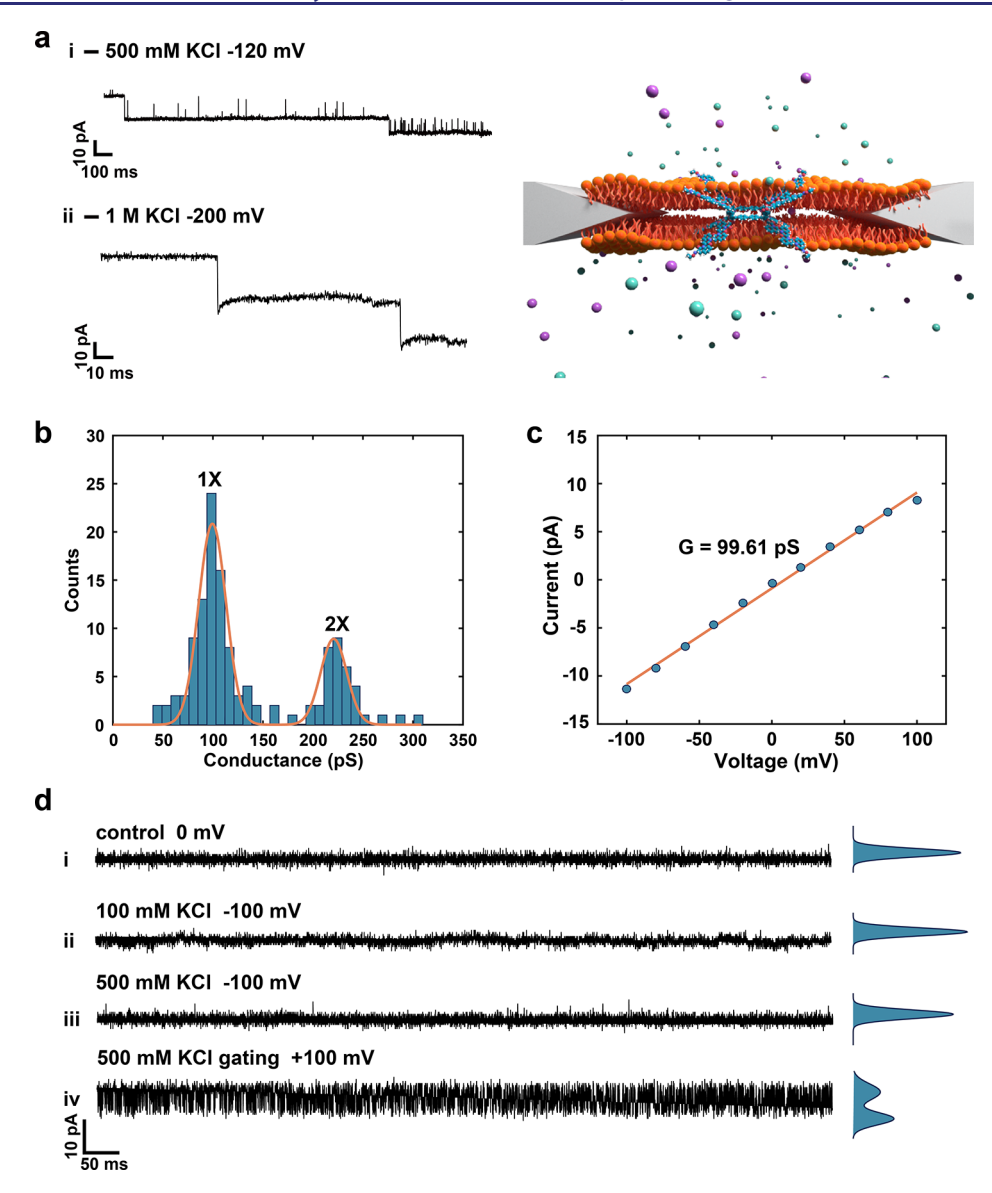


Figure 2. Single channel recordings of ion transport through individual EPM nanopores. (a) Stepwise incorporation of individual EPM nanopores into lipid bilayers. (b) Histogram of channel conductance obtained from 127 single-step incorporation events in 500 mM KCl. Conductance of the first fit peak $(1\times)$ and of the second fit peak $(2\times)$ is 99.28 ± 1.95 and 220.5 ± 4.40 pS, respectively. The value of the first fit peak represents the conductance of the nanopore formed by a single EPM molecule. Error bars are derived from the Gaussian fitting. (c) Current—voltage characteristic of a single EPM nanopore in 500 mM KCl. (d) Typical current traces and normalized current histograms (right) of individual EPM nanopores, and the gating behavior. The normalized histogram of the current trajectories generated by the stable nanopores is unimodal. The normalized histogram of the current trajectory with gating behavior is bimodal, indicating that the nanopore switches between two conductance states.

functionalities. Figure 3e reveals a diode-like ionic current rectification of an EPM nanopore operating under asymmetric condition of 1 M KCl/1 M NaCl. In addition, measurements from a mixture of KCl and NaCl solutions suggest that the selectivity can be precisely regulated by the mole fraction control of the mixed solution (Figure 3f and Figure S14). Thus, our single pore measurements quantitatively demonstrate that EPM nanopores exhibit high potassium selectivity, which is comparable to the reported selectivity of crown etherbased artificial potassium channels^{35–38} and foldamer-based channel³⁹ but is still lower than the highest reported selectivity of natural potassium channel KcsA.^{34,40}

The physical principle governing the operation of our synthetic potassium channel remains elusive at the atomic level. One primary challenge lies in characterizing the *in situ*

conformation of the EPM pore in a lipid membrane, which can differ from its known crystal structure. ²³ Although we have successfully identified the chemical structures using various analytical tools, the dynamic EPM configuration in a lipid bilayer remains largely unknown. We thereby optimized the spatial structures of EPM using the density functional theory (DFT) calculations to minimize the free energy under virtual conditions (Figure S15). Referring to the literature, ^{1,3} ion bindings play an important role in selective transport. Moderate ion binding can facilitate the selective transport *via* compensating the dehydration cost whereas tight bindings due to deep potential wells can trap the ions and prohibit the conduction. ^{1,41,42} Our NMR and MALDI-TOF characterizations suggest that the binding of sodium ion to our macrocycle structures is preferable (Figures S16–S19). To

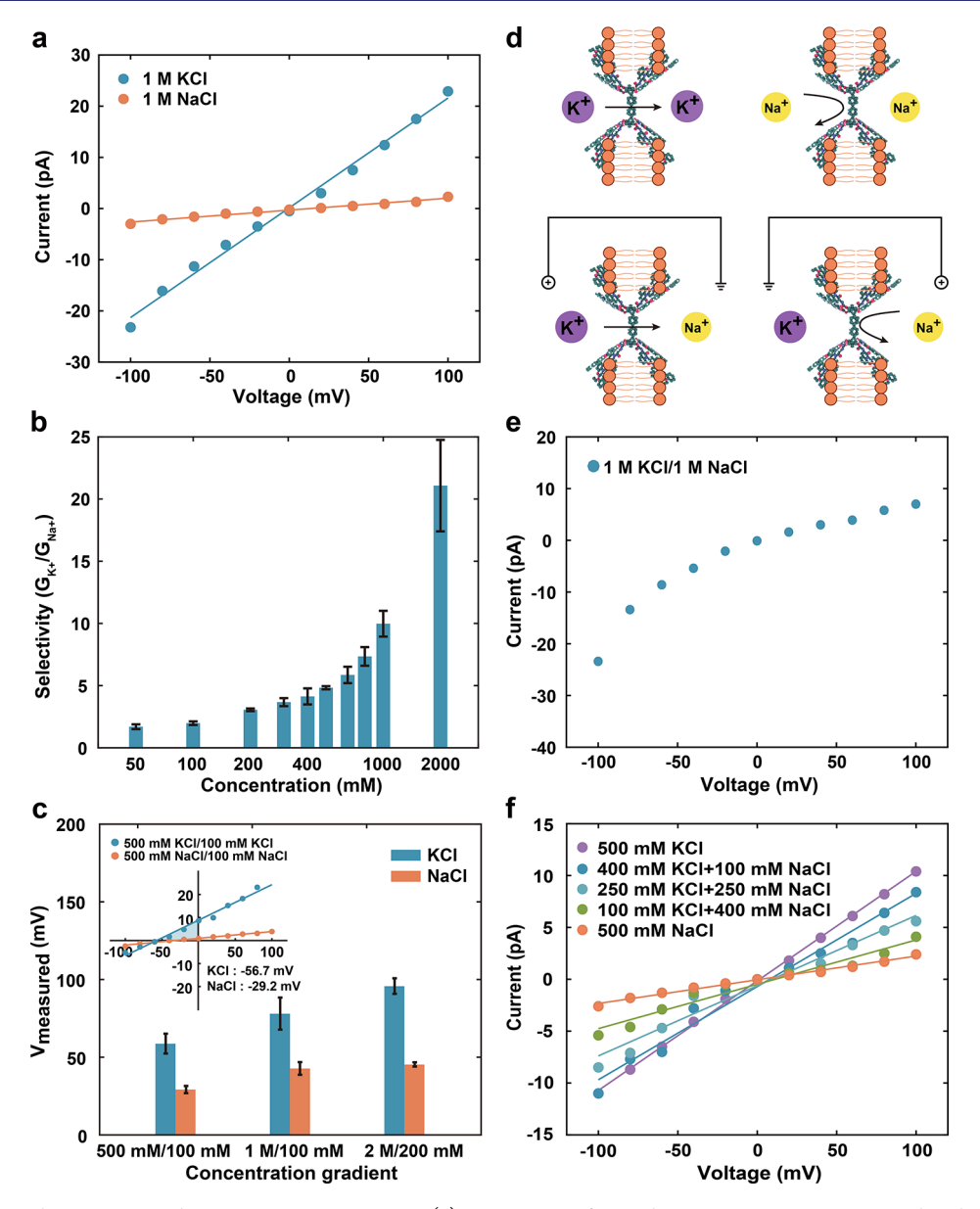


Figure 3. Potassium-selective ion conduction in EPM nanopores. (a) I-V curves of a single EPM nanopore in 1 M KCl and 1 M NaCl solution. Blue: KCl solution. Orange: NaCl solution. (b) Selectivity of the EPM nanopores as a function of ion concentrations. The selectivity factor is the ratio between potassium conductance and sodium conductance under the same concentration. (c) Reverse potential in three experiments with different concentration gradients. Inset: I-V curves obtained under the concentration gradient in 500 mM/100 mM KCl and NaCl solution. Blue: KCl solution. Orange: NaCl solution. Error bars are derived from the standard deviation from multiple experimental measurements. (d) Schematic diagram for the transport of potassium and sodium ions in a single EPM nanopore. (e) I-V curves of asymmetric solution in 1 M KCl/1 M NaCl solution. (f) Ionic current measurements in the mixtures of KCl and NaCl solution for EPM nanopore. The total ionic strength is 500 mM.

provide a connection between the ion binding results and the molecular-level physical image, we used the candidates obtained from the DFT calculations for molecular dynamics (MD) simulations of ion transport.

From the standpoint of the MD method, the highly reproducible, stable, and selective ion transport through EPM nanopore is somewhat of an enigma. Following the methods used previously to simulate various synthetic nanopore systems, ^{8,25,43} we built a computational model that included a single EPM nanopore embedded in a lipid bilayer membrane and surrounded by 1 M electrolyte solution, Figure 4a. In a typical simulation, the EPM nanopore remained stably embedded in the lipid bilayer while the electrolyte solution developed two funnel-like protrusions reaching toward the

nanopore constriction, Figure 4a. During the simulation, water molecules were observed to form a continuous path from one side of the membrane to the other, allowing water to pass stochastically across the pore, Figure 4b, with the rate (~3 molecules/ns) expected for a similar size biological nanopore. The structural fluctuations in the pillararene molecule were confined to less than 2.5 Å average root mean squared deviation (Figure S20). The peptide side chains that extended radially from the constriction in the initial model (Figure 1) adopted a more compact conformation at the end of the unrestrained equilibration simulation, Figure 4c. Applied electric field simulations, however, produced mixed results: the ionic conduction was found to depend much stronger on

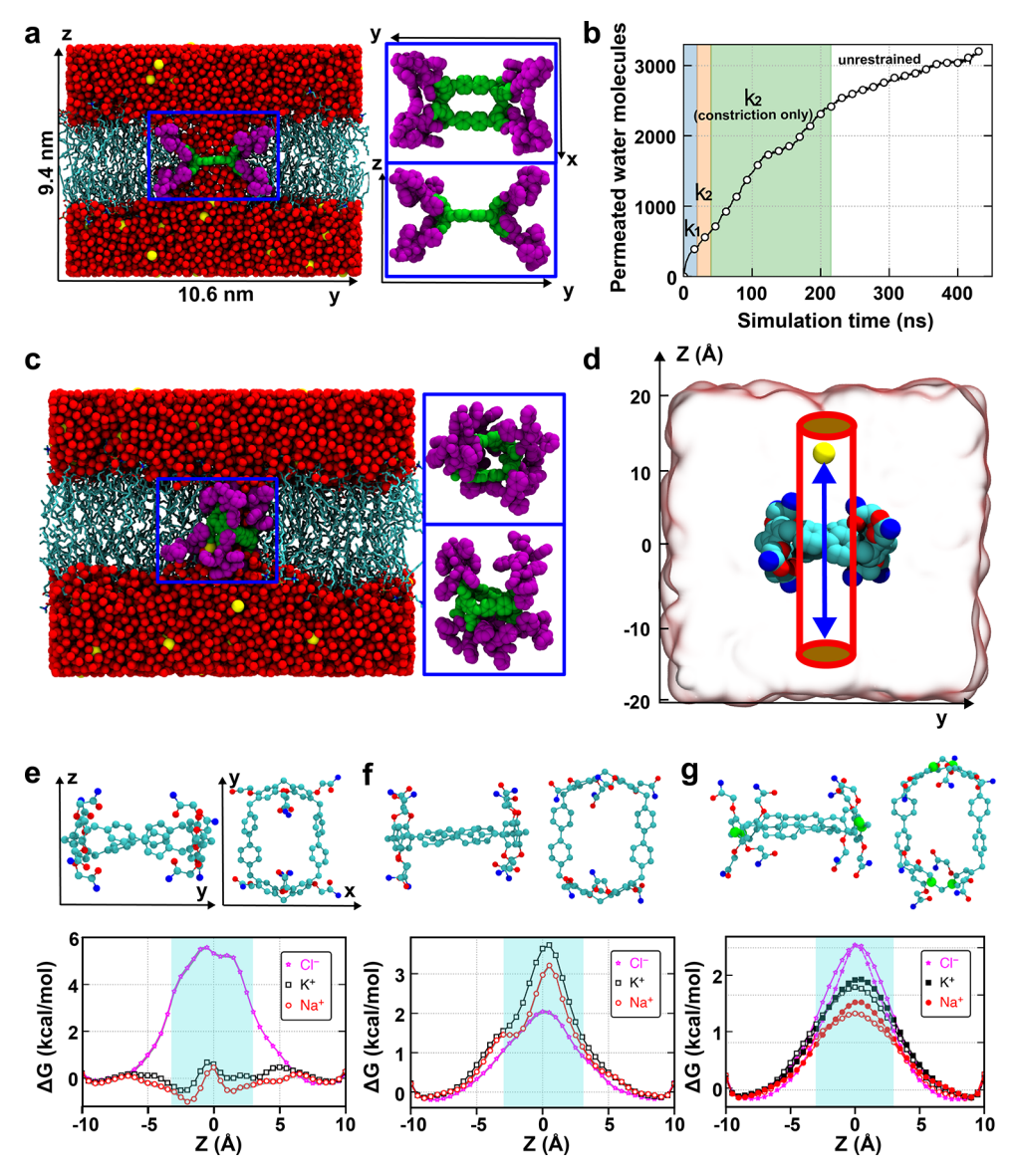


Figure 4. All-atom MD simulations of water and ion transport through EPM nanopores. (a) Cut-away view of the initial all-atom model of EPM nanopore embedded in a POPC bilayer and solvated with 1 M KCl electrolyte. The constriction region of the channel is shown using green spheres, whereas the peptide side chains are shown in purple. The oxygen atom of the water molecules is shown using red spheres. The K^+ and Cl^- ions are shown using yellow and cyan spheres, whereas the lipid bilayer is shown using the thick turquoise line. The initial configuration of the EPM channel (top and side view) is shown in the right panels. (b) Number of water molecules permeated through the EPM channel as a function of the simulation time. The shaded regions indicate the time intervals when harmonic restraints were applied to all atoms of the EPM nanopore (with k_1 and k_2 of 1 and 0.1 kcal $mol^{-1} \text{ Å}^{-2}$, respectively) and only to the atoms of the nanopore constriction (k_3 = 0.1 kcal $mol^{-1} \text{ Å}^{-2}$). (c) Microscopic configuration of the simulation system at the end of the 450 ns MD simulation. (d) Schematics for the calculations of the ion permeating across the EPM channel, showing a typical snapshot of EPM nanopore immersed in a box of water and ions. The respective ion is confined to the cylindrical region (radius 3 Å) around the nanopore. (e-g) Free energy (PMF) of the K^+ , Na^+ , and Cl^- ions as a function of the distance from the center of the EPM channel along the z-axis computed having all heavy atoms of the EPM restrained to either DFT-optimized (e) or crystallographic (f) structures or having only the four carbon atoms (orange) restrained (g). The two curves for each ion type in panel (g) were obtained using the DFT-optimized and crystallographic structures as starting configurations for the free-energy calculations.

the structure of the interface between the lipid bilayer and the EPM nanopore than on the electrolyte type.

To take away the effect of the unknown structure of the lipid—nanopore junction, we built a simulation system containing only the constriction of the EPM nanopore, Figure 4d, and used replica exchange umbrella sampling simulations to evaluate the energetics of ion passage. The resulting potential of mean force (PMF) was found to indicate considerable ion selectivity; however, the specific effect varied greatly upon minute changes to the constriction configuration,

Figure 4e-g. Another limiting factor is that the current molecular force field has not been parametrized to fully reproduce specific binding of cations to aromatic residues. ^{33,44} Taken together, our MD simulations failed to find one stable microscopic configuration of the EPM nanopore/lipid bilayer system that would reproduce all the experimental observations. Our analysis, however, showed that the nanopore constriction itself can be potassium selective and that such selectivity sensitively depends on the arrangement of individual atoms within the constriction (Figure 4e). A possible reconciliation of

the simulation and experimental data could be a picture where the EPM nanopore indeed undergoes rapid conformational changes but those changes are too rapid to be registered experimentally, producing the ionic current that, just like the light of a fluorescent bulb, appears steady at a longer (milliseconds) time scale but is inherently bursty when looked with a finer temporal resolution.

CONCLUSION

Macrocycle nanopores are ideally designed for atomic-precision ionic and molecular transport measurements. Here, we demonstrated the successful construction of a stable, single transmembrane EPM nanopore and explored its potassium-selective ion transport properties. Compared with the recently reported nanopore strategies using polymer folding ¹³ and *de novo* design of protein pores, ⁴⁵ our macrocycle nanopores directly benefit from the precisely programmed molecular geometry and functionalities. Considering the single unit thickness, this class of nanopores has the potential to deliver an ultrahigh sensitivity in nanopore experiments. Future studies exploring larger organic macrocycles (Table 1) may also enable novel applications in DNA and protein sensing.²⁷

ASSOCIATED CONTENT

Supporting Information

The Supporting Information is available free of charge at https://pubs.acs.org/doi/10.1021/jacs.1c04910.

Chemical synthesis and characterization of EPM nanopores, experimental setup, ion transport measurements and methods, optimization of EPM structures, all-atom MD simulations of water and ion transport through EPM nanopores, supporting discussions and figures, supporting movie legends, supporting references (PDF) Rotating view of the EPM molecule illustrating the 3D structure of the nanopore (MP4)

All-atom MD simulations of the EPM nanopore embedded in the POPC lipid bilayer membrane and solvated in a box of water and ions (MP4)

AUTHOR INFORMATION

Corresponding Authors

Aleksei Aksimentiev — Department of Physics, University of Illinois at Urbana—Champaign, Urbana, Illinois 61801, United States; orcid.org/0000-0002-6042-8442; Email: aksiment@illinois.edu

Jiandong Feng — Laboratory of Experimental Physical Biology, Department of Chemistry, Zhejiang University, Hangzhou 310027, China; orcid.org/0000-0002-2143-3986; Email: jiandong.feng@zju.edu.cn

Authors

Dan Qiao – Laboratory of Experimental Physical Biology, Department of Chemistry, Zhejiang University, Hangzhou 310027, China

Himanshu Joshi — Department of Physics, University of Illinois at Urbana—Champaign, Urbana, Illinois 61801, United States; orcid.org/0000-0003-0769-524X

Huangtianzhi Zhu — State Key Laboratory of Chemical Engineering, Key Laboratory of Excited-State Materials of Zhejiang Province, Stoddart Institute of Molecular Science, Department of Chemistry, Zhejiang University, Hangzhou 310027, China; orcid.org/0000-0002-1271-6415

- Fushi Wang Laboratory of Experimental Physical Biology, Department of Chemistry, Zhejiang University, Hangzhou 310027. China
- Yang Xu Laboratory of Experimental Physical Biology, Department of Chemistry, Zhejiang University, Hangzhou 310027. China
- Jia Gao Laboratory of Experimental Physical Biology, Department of Chemistry, Zhejiang University, Hangzhou 310027, China

Feihe Huang — State Key Laboratory of Chemical Engineering, Key Laboratory of Excited-State Materials of Zhejiang Province, Stoddart Institute of Molecular Science, Department of Chemistry, Zhejiang University, Hangzhou 310027, China; ZJU-Hangzhou Global Scientific and Technological Innovation Center, Hangzhou 311215, China; orcid.org/0000-0003-3177-6744

Complete contact information is available at: https://pubs.acs.org/10.1021/jacs.1c04910

Author Contributions

*D.Q. and H.J. contributed equally to this work.

The authors declare no competing financial interest.

ACKNOWLEDGMENTS

This study was funded by the Natural Science Foundation of Zhejiang Province (LR20B050002), the National Natural Science Foundation of China (21974123), the National Key R&D Program of China (2020YFA0211200), the Fundamental Research Funds for the Central Universities, China (2019XZZX003-01), and the Hundreds Program of Zhejiang University. A.A. and H.J. acknowledge support from the National Science Foundation of USA (DMR-1827346) and the supercomputer time provided through the XSEDE allocation grant (MCA05S028) and the Leadership Resource Allocation MCB20012 on Frontera of the Texas Advanced Computing Center. We also thank the Center of Analytical Service at Zhejiang University for help with MALDI-TOF measurements and the Cryo-EM Center at Zhejiang University for access to TEM.

REFERENCES

- (1) DeMarco, K. R.; Bekker, S.; Vorobyov, I. Challenges and advances in atomistic simulations of potassium and sodium ion channel gating and permeation. *J. Physiol.* **2019**, *597* (3), *679*–*698*.
- (2) Doyle, D. A.; Cabral, J. M.; Pfuetzner, R. A.; Kuo, A.; Gulbis, J. M.; Cohen, S. L.; Chait, B. T.; MacKinnon, R. The Structure of the Potassium Channel: Molecular Basis of K+ Conduction and Selectivity. *Science* **1998**, 280 (5360), 69–77.
- (3) Gouaux, E.; MacKinnon, R. Principles of Selective Ion Transport in Channels and Pumps. *Science* **2005**, *310*, 1461–1465.
- (4) Xue, L.; Yamazaki, H.; Ren, R.; Wanunu, M.; Ivanov, A. P.; Edel, J. B. Solid-state nanopore sensors. *Nature Reviews Materials* **2020**, *5*, 931–951.
- (5) Hu, Z. L.; Huo, M. Z.; Ying, Y. L.; Long, Y. T. Biological Nanopore Approach for Single-Molecule Protein Sequencing. *Angew. Chem.* **2021**, *133*, 14862–14873.
- (6) Epsztein, R.; DuChanois, R. M.; Ritt, C. L.; Noy, A.; Elimelech, M. Towards single-species selectivity of membranes with subnanometre pores. *Nat. Nanotechnol.* **2020**, *15* (6), 426–436.
- (7) Howorka, S. Building membrane nanopores. *Nat. Nanotechnol.* **2017**, *12*, 619–630.
- (8) Song, W.; Joshi, H.; Chowdhury, R.; Najem, J. S.; Shen, Y.-x.; Lang, C.; Henderson, C. B.; Tu, Y.-M.; Farell, M.; Pitz, M. E.;

- Maranas, C. D.; Cremer, P. S.; Hickey, R. J.; Sarles, S. A.; Hou, J.-l.; Aksimentiev, A.; Kumar, M. Artificial water channels enable fast and selective water permeation through water-wire networks. *Nat. Nanotechnol.* **2020**, *15* (1), 73–79.
- (9) Shen, J.; Fan, J.; Ye, R.; Li, N.; Mu, Y.; Zeng, H. Polypyridine-Based Helical Amide Foldamer Channels: Rapid Transport of Water and Protons with High Ion Rejection. *Angew. Chem., Int. Ed.* **2020**, *59* (32), 13328–13334.
- (10) Feng, J.; Graf, M.; Liu, K.; Ovchinnikov, D.; Dumcenco, D.; Heiranian, M.; Nandigana, V.; Aluru, N. R.; Kis, A.; Radenovic, A. Single-layer MoS₂ nanopores as nanopower generators. *Nature* **2016**, 536 (7615), 197–200.
- (11) Tunuguntla, R. H.; Henley, R. Y.; Yao, Y. C.; Pham, T. A.; Wanunu, M.; Noy, A. Enhanced water permeability and tunable ion selectivity in subnanometer carbon nanotube porins. *Science* **2017**, 357 (6353), 792–796.
- (12) Langecker, M.; Arnaut, V.; Martin, T. G.; List, J.; Renner, S.; Mayer, M.; Dietz, H.; Simmel, F. C. Synthetic Lipid Membrane Channels Formed by Designed DNA Nanostructures. *Science* **2012**, 338 (6109), 932–936.
- (13) Jiang, T.; Hall, A.; Eres, M.; Hemmatian, Z.; Qiao, B.; Zhou, Y.; Ruan, Z.; Couse, A. D.; Heller, W. T.; Huang, H.; de la Cruz, M. O.; Rolandi, M.; Xu, T. Single-chain heteropolymers transport protons selectively and rapidly. *Nature* **2020**, *577* (7789), 216–220.
- (14) Huang, W. L.; Wang, X. D.; Ao, Y. F.; Wang, Q. Q.; Wang, D. X. Artificial Chloride-Selective Channel: Shape and Function Mimic of the ClC Channel Selective Pore. *J. Am. Chem. Soc.* **2020**, *142* (31), 13273–13277.
- (15) Tanaka, Y.; Kobuke, Y.; Sokabe, M. A Non-Peptidic Ion Channel with K+ Selectivity. *Angew. Chem., Int. Ed. Engl.* **1995**, 34 (6), 693–694.
- (16) Sakai, N.; Matile, S. Synthetic ion channels. *Langmuir* **2013**, 29 (29), 9031–9040.
- (17) Si, W.; Xin, P.; Li, Z. T.; Hou, J. L. Tubular unimolecular transmembrane channels: construction strategy and transport activities. *Acc. Chem. Res.* **2015**, 48 (6), 1612–1619.
- (18) Xin, P.; Kong, H.; Sun, Y.; Zhao, L.; Fang, H.; Zhu, H.; Jiang, T.; Guo, J.; Zhang, Q.; Dong, W. Artificial K⁺ Channels Formed by Pillararene-Cyclodextrin Hybrid Molecules: Tuning Cation Selectivity and Generating Membrane Potential. *Angew. Chem., Int. Ed.* **2019**, *58* (9), 2779–2784.
- (19) Si, W.; Li, Z. T.; Hou, J. L. Voltage-Driven Reversible Insertion into and Leaving from a Lipid Bilayer: Tuning Transmembrane Transport of Artificial Channels. *Angew. Chem., Int. Ed.* **2014**, 53 (18), 4578–4581.
- (20) Fang, A.; Kroenlein, K.; Riccardi, D.; Smolyanitsky, A. Highly mechanosensitive ion channels from graphene-embedded crown ethers. *Nat. Mater.* **2019**, *18* (1), 76–81.
- (21) Acar, E. T.; Buchsbaum, S. F.; Combs, C.; Fornasiero, F.; Siwy, Z. S. Biomimetic potassium-selective nanopores. *Science Advances* **2019**, *5* (2), No. eaav2568.
- (22) Ogoshi, T.; Yamagishi, T.; Nakamoto, Y. Pillar-Shaped Macrocyclic Hosts Pillar[n]arenes: New Key Players for Supramolecular Chemistry. *Chem. Rev.* **2016**, *116* (14), 7937–8002.
- (23) Gao, B.; Tan, L. L.; Song, N.; Li, K.; Yang, Y. W. A high-yield synthesis of [m]biphenyl-extended pillar[n]arenes for an efficient selective inclusion of toluene and m-xylene in the solid state. *Chem. Commun.* **2016**, 52 (34), 5804–5807.
- (24) Chen, L.; Si, W.; Zhang, L.; Tang, G.; Li, Z. T.; Hou, J. L. Chiral Selective Transmembrane Transport of Amino Acids through Artificial Channels. *J. Am. Chem. Soc.* **2013**, *135* (6), 2152–2155.
- (25) Göpfrich, K.; Li, C. Y.; Mames, I.; Bhamidimarri, S. P.; Ricci, M.; Yoo, J.; Mames, A.; Ohmann, A.; Winterhalter, M.; Stulz, E.; Aksimentiev, A.; Keyser, U. F. Ion Channels Made from a Single Membrane-Spanning DNA Duplex. *Nano Lett.* **2016**, *16* (7), 4665–4669
- (26) Burns, J. R.; Seifert, A.; Fertig, N.; Howorka, S. A biomimetic DNA-based channel for the ligand-controlled transport of charged

- molecular cargo across a biological membrane. *Nat. Nanotechnol.* **2016**, *11*, 152–156.
- (27) Ayub, M.; Bayley, H. Engineered transmembrane pores. Curr. Opin. Chem. Biol. 2016, 34, 117–126.
- (28) Degiacomi, M. T.; Iacovache, I.; Pernot, L.; Chami, M.; Kudryashev, M.; Stahlberg, H.; Van Der Goot, F. G.; Dal Peraro, M. Molecular assembly of the aerolysin pore reveals a swirling membrane-insertion mechanism. *Nat. Chem. Biol.* **2013**, *9* (10), 623–629.
- (29) Cressiot, B.; Greive, S. J.; Si, W.; Pascoa, T. C.; Mojtabavi, M.; Chechik, M.; Jenkins, H. T.; Lu, X.; Zhang, K.; Aksimentiev, A.; Antson, A. A.; Wanunu, M. Porphyrin-Assisted Docking of a Thermophage Portal Protein into Lipid Bilayers: Nanopore Engineering and Characterization. ACS Nano 2017, 11 (12), 11931–11945.
- (30) Spruijt, E.; Tusk, S. E.; Bayley, H. DNA scaffolds support stable and uniform peptide nanopores. *Nat. Nanotechnol.* **2018**, *13* (8), 739–745.
- (31) Geng, J.; Kim, K.; Zhang, J.; Escalada, A.; Tunuguntla, R.; Comolli, L. R.; Allen, F. I.; Shnyrova, A. V.; Cho, K. R.; Munoz, D.; Wang, Y. M.; Grigoropoulos, C. P.; Ajo-Franklin, C. M.; Frolov, V. A.; Noy, A. Stochastic transport through carbon nanotubes in lipid bilayers and live cell membranes. *Nature* **2014**, *514* (7524), *612*–*615*.
- (32) Hille, B., Chapter 14 Selective permeability: Independence. In *Ion Channels of Excitable Menbranes*, 3rd ed.; Sinauer Associates, 2001; pp 445–450.
- (33) Kumpf, R. A.; Dougherty, D. A. A mechanism for ion selectivity in potassium channels: computational studies of cation-pi interactions. *Science* **1993**, *261* (5129), 1708–1710.
- (34) Shrivastava, I. H.; Peter Tieleman, D.; Biggin, P. C.; Sansom, M. S. P. K⁺ versus Na⁺ Ions in a K Channel Selectivity Filter: A Simulation Study. *Biophys. J.* **2002**, *83* (2), *633*–645.
- (35) Gilles, A.; Barboiu, M. Highly selective artificial K⁺ channels: an example of selectivity-induced transmembrane potential. *J. Am. Chem. Soc.* **2016**, *138* (1), 426–432.
- (36) Li, Y. H.; Zheng, S.; Legrand, Y. M.; Gilles, A.; Van der Lee, A.; Barboiu, M. Structure-Driven Selection of Adaptive Transmembrane Na⁺ Carriers or K⁺ Channels. *Angew. Chem., Int. Ed.* **2018**, *57* (33), 10520–10524.
- (37) Zheng, S. p.; Huang, L. B.; Sun, Z.; Barboiu, M. Self-Assembled Artificial Ion-Channels toward Natural Selection of Functions. *Angew. Chem., Int. Ed.* **2021**, *60*, 566–597.
- (38) Sun, Z.; Gilles, A.; Kocsis, I.; Legrand, Y. M.; Petit, E.; Barboiu, M. Squalyl Crown Ether Self-Assembled Conjugates: An Example of Highly Selective Artificial K⁺ Channels. *Chem. Eur. J.* **2016**, 22 (6), 2158–2164.
- (39) Qi, S.; Zhang, C.; Yu, H.; Zhang, J.; Yan, T.; Lin, Z.; Yang, B.; Dong, Z. Foldamer-Based Potassium Channels with High Ion Selectivity and Transport Activity. *J. Am. Chem. Soc.* **2021**, *143* (9), 3284–3288.
- (40) LeMasurier, M.; Heginbotham, L.; Miller, C. Kcsalt's a Potassium Channel. J. Gen. Physiol. 2001, 118 (3), 303-314.
- (41) Berezhkovskii, A. M.; Bezrukov, S. M. Optimizing transport of metabolites through large channels: molecular sieves with and without binding. *Biophys. J.* **2005**, 88 (3), L17–L19.
- (42) Chen, F.; Gu, Z.; Zhao, C.; Chen, Y.; Jiang, X.; He, Z.; Lu, Y.; Zhou, R.; Feng, J. Ionic conductance oscillations in sub-nanometer pores probed by optoelectronic control. *Matter* **2021**, *4*, 2378–2391.
- (43) Shen, Y.; Si, W.; Erbakan, M.; Decker, K.; De Zorzi, R.; Saboe, P. O.; Kang, Y. J.; Majd, S.; Butler, P. J.; Walz, T.; Aksimentiev, A.; Hou, J. L.; Kumar, M. Highly permeable artificial water channels that can self-assemble into two-dimensional arrays. *Proc. Natl. Acad. Sci. U. S. A.* **2015**, *112* (32), 9810–9815.
- (44) Liu, H.; Fu, H.; Shao, X.; Cai, W.; Chipot, C. Accurate Description of Cation- π Interactions in Proteins with a Non-polarizable Force Field at No Additional Cost. *J. Chem. Theory Comput.* **2020**, *16* (10), 6397–6407.
- (45) Xu, C.; Lu, P.; Gamal El-Din, T. M.; Pei, X. Y.; Johnson, M. C.; Uyeda, A.; Bick, M. J.; Xu, Q.; Jiang, D.; Bai, H.; Reggiano, G.; Hsia, Y.; Brunette, T. J.; Dou, J.; Ma, D.; Lynch, E. M.; Boyken, S. E.;

Huang, P. S.; Stewart, L.; DiMaio, F.; Kollman, J. M.; Luisi, B. F.; Matsuura, T.; Catterall, W. A.; Baker, D. Computational design of transmembrane pores. *Nature* **2020**, 585 (7823), 129–134.

1